

# Learning-Based Fingertip Force Estimation for Soft Wearable Hand Robot With Tendon-Sheath Mechanism

Brian Byunghyun Kang <sup>1</sup>, Daekyum Kim <sup>1</sup>, Hyungmin Choi <sup>1</sup>, Useok Jeong <sup>1</sup>, Kyu Bum Kim, Sungho Jo <sup>2</sup>, and Kyu-Jin Cho <sup>1</sup>

**Abstract**—Soft wearable hand robots with tendon-sheath mechanisms are being actively developed to assist people with lost hand mobility. For these robots, accurately estimating fingertip forces leads to successful object grasping. An approach can utilize information from actuators assuming quasi-static environments. However, non-linearity and hysteresis with regards to the dynamic changes of the tendon-sheath mechanism hinder accurate fingertip force estimation. This paper proposes a learning-based method to estimate fingertip forces by integrating dynamic information of motor encoders, wire tension, and sheath bending angles. The model is modified from Long Short-Term Memory by incorporating a residual term that governs the dynamic changes in sheath bending angles. Using a tendon-driven soft wearable hand robot, the proposed model obtained RMSE less than 0.44 N. It was further evaluated under criteria ranging from different object sizes, bending angle ranges, and forces. Finally, a repeatability test (0.46 N in RMSE), real-time applicability (125 Hz), and force control (12.7% in MAPE) were performed to verify the feasibility of the proposed method.

**Index Terms**—Soft robot applications, wearable robots, modeling, control, and learning for soft robots.

## I. INTRODUCTION

RECENTLY, various wearable hand robots made by soft materials have been developed to assist people with full or partial loss of hand mobility [1]–[10]. These soft wearable hand robots are mostly actuated either by using pneumatic actuation-based [1], [2] or tendon-driven systems [3]–[10]. When using the tendon-driven actuation system, soft wearable hand robots, in general, are composed of a glove (wearing part), an actuation

Manuscript received September 10, 2019; accepted January 1, 2020. Date of publication January 13, 2020; date of current version January 30, 2020. This letter was recommended for publication by Associate Editor H. Andreasson and Editor S. Behnke upon evaluation of the reviewers' comments. This work was supported by the National Research Foundation of Korea Grant funded by the Korean Government (MSIT) under Grants NRF-2016R1A5A1938472 and NRF-2019R1F1A1041277. (B. B. Kang and D. Kim contributed equally to this work.) (Corresponding author: Kyu-Jin Cho and Sungho Jo.)

B. B. Kang, H. Choi, K. B. Kim, and K.-J. Cho are with the Biorobotics Laboratory, Department of Mechanical Engineering, IAMD, Seoul National University, Seoul 08826, Korea (e-mail: brianbkang@snu.ac.kr; tndhals@snu.ac.kr; kbum34@snu.ac.kr; kjcho@snu.ac.kr).

D. Kim and S. Jo are with the Neuro-Machine Augmented Intelligence Laboratory, School of Computing, KAIST, Daejeon 305-701, Korea (e-mail: daekyum@kaist.ac.kr; shjo@kaist.ac.kr).

U. Jeong is with the Robotics R&D Group, Korea Institute of Industrial Technology (KITECH), Hangeul-ro 143, Sangnok-gu, Ansan-si 15588, Korea (e-mail: usjeong@kitech.re.kr).

Digital Object Identifier 10.1109/LRA.2020.2966391

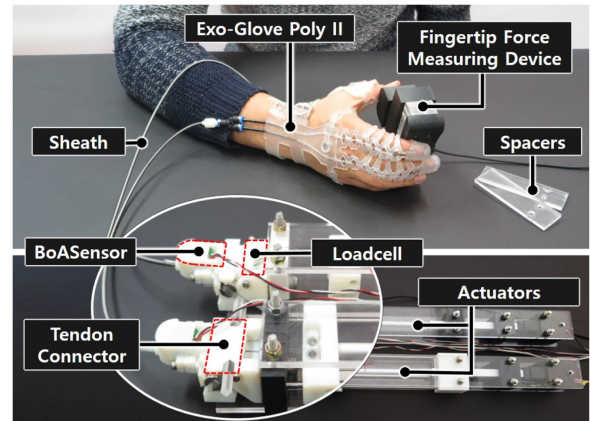


Fig. 1. System overview.

system, and a tendon-sheath mechanism (TSM) [3]–[10]. The TSM, the connecting component located between the glove and the actuation system, plays two important roles in tendon-driven soft wearable hand robots: 1) transmission of the power from the motor to the glove and 2) glove weight reduction via separation of the actuation system from the glove. These benefits enable increased portability of soft wearable hand robots, potentially allowing the assistance of various daily tasks.

Up until now, the trend has been to utilize under-actuation as a characteristic for TSM when making soft wearable hand robots for the assistance of Activities of Daily Livings (ADLs). [3]–[8]. The under-actuated system is to intentionally provide lower degree of freedom for the robots in order to deploy the fewer number of actuators. Such system has its merits in that it minimizes the complexity of the actuation, thus providing compactness and portability to the robots. Due to the limited number of actuators, robots with under-actuated systems have focused on generating or supporting a simple uniform grasp motion.

For the wearable hand robots to be appropriately utilized in daily life, it is important to generate proper grasping forces in accordance with various object characteristics. In other words, grasping performance depends on generating adequate grasping forces. For instance, to hold a basketball, which is an object relatively larger than a hand, the human applies an adequate grasping force rather than overcompensating with a maximum grasping force. Thus, it is essential for the robot to acquire fingertip information when exerting forces to the target object.

To obtain fingertip forces between the fingers and the object, one intuitive solution is to use a tactile sensor on a fingertip. Previous studies have suggested various types of tactile sensors that have potential to be used in wearable hand robot applications [11]–[13]. Wang *et al.* proposed a three-axis flexible tactile sensor array based on conductive rubber [13]. Cheng *et al.* proposed a fabric-based pneumatic sensor for bending angles and contact force detection [2]. Unlike sensors using soft materials, wearable finger sensor modules utilizing various types of sensors were also developed [14]–[16]. Besides studies related to sensors, soft wearable hand robots with embedded sensors are developed for various applications including rehabilitation, assisting repetitive tasks, and haptics [2], [8], [17], [18]. However, sensors on the glove can limit the wearable hand robots to assist ADLs for people with sensorimotor impairment. Placing sensors on the glove not only increase the size of the robot but also result in individual calibration. This is due to the fact that the placement of the sensors are user dependent. Furthermore, electric components including sensors can endanger users when performing ADLs in water-aqueous activities like dish washing or tooth brushing.

As an alternative approach, fingertip forces can possibly be estimated by utilizing information obtained from the actuation system with the TSM. The major issue in this approach is sheath non-linearity cause by bending and friction. Conventionally, the capstan formula has been used to describe frictional non-linearity [19] and has been adopted as a tension estimation model output of TSM [20]–[22]. Li *et al.* presented a preliminary study using deep learning [23] to predict the frictional hysteresis of TSM in the endoscopic device under the fixed shape of the sheath. Jeong *et al.* proposed BoASensor to handle frictional hysteresis of TSM by measuring sheath bending angles in real-time [24]–[26]. Although those studies demonstrated the effectiveness of force estimation when using TSMs under certain environments, several limitations still impede the actual application in uncontrolled environments. While existing studies assume quasi-static environments, in the case of soft wearable hand robots, the dynamic change of sheath bending angles is a key concern. During a reaching-grasping sequence of actions, sheath bending angles are not constant, resulting in changing fingertip forces. Another issue is non-linearity caused by the compliance of the soft wearable hand robot and human hand. These issues in sum make it hard to estimate fingertip forces by existing methods.

This letter proposes a learning-based approach to estimate fingertip forces without any tactile sensors by integrating information from motor encoders, wire tension, and sheath bending angles for soft wearable hand robots with the TSM. Assuming the contact force is generated only at the fingertips, the proposed approach can estimate fingertip forces regardless of variation of object sizes and dynamic change in sheath bending angles. In order to realize the proposed approach, Exo-Glove Poly II [5], [6], an under-actuated soft wearable hand robot with the TSM, was modified to integrate BoASensors [24]–[26] with the actuation system as depicted in Fig. 1. For collecting datasets, motor encoders and wire tension were measured from the actuation system while sheath bending angles were measured from BoASensor. Bending Time-gradient Long-Short Term Memory (BT-LSTM), a modified version of Long-Short Term Memory (LSTM [27]), is proposed to deal with obtained non-linear information obtained from the TSM. BT-LSTM has a residual structure that inputs bending-time gradient, which incorporates

with the hidden outputs of LSTM. Adding this structure enables to better deal with the dynamic changes of the angle displacement. Performances of BT-LSTM were compared with conventional learning algorithms to estimate fingertip forces for various object sizes and sheath bending angles for verification. Considering sheaths movements during grasping motions, the performance of the model was evaluated by estimating fingertip forces under the dynamic change of sheath bending angles. In addition, a repeatability test, real-time applicability, and force control experiment were performed to verify the feasibility of the proposed method in real-life application.

Section II addresses issues related to estimating fingertip forces in soft wearable hand robot with TSM. Section III explains overall hardware system configuration and proposed algorithm. In Section IV, experimental results are presented and analyzed. Lastly, Section V concludes the paper with discussions and future works.

## II. PROBLEM DESCRIPTION

### A. Problem Definition

The objective of this study is to estimate fingertip forces of an under-actuated soft wearable hand robot with TSM using a machine learning algorithm. Instead of directly attaching sensors onto the glove, motor encoders, flexion wire tension and sheath bending angles are used as an input of the machine learning model. There are some complications when modeling fingertip forces from the given parameters, like non-linearity and hysteresis. As a major factor that complicates fingertip force estimation, the non-linear relationship between these parameters can be represented as two aspects: 1) non-linearity in the robot system and 2) non-linearity caused by the environment. The first includes friction in TSM, compliance of TSM, and compliance of the glove. The second aspect includes compliance of a user hand, variation in hand sizes, variation of target object sizes, and variation of target object stiffness. To clearly address the concept of non-linear and hysteresis behaviors in the soft wearable hand robot with TSM, relationships between actuation lengths, flexion wire tension, and fingertip forces are plotted in Fig. 2. Among these factors, this study focuses on estimating fingertip forces considering sheath angle variation and object size variation. For the system with TSM, considering the non-linear tendon behavior caused by the sheath angle variation (Fig. 3) is critical for estimating and controlling the system.

### B. Nonlinear Behaviors Between Parameters

1) *Varying Objects*: Fig. 2(a)–(c) show nonlinear behaviors between parameters according to different object sizes when the sheath bending angle and the actuation length are fixed. For comparison, three cases are plotted: grasping without an object (No object), grasping an 68 mm (Medium object) and 93 mm (Large object) objects. Fig. 2(a) shows non-linear trends between actuation lengths and flexion wire tension. Obviously, wire tension for larger objects tends to increase faster and to have the higher value when reaching the peak point. “No object” case was included to show the performance of the robot without any object as a reference. Fig. 2(b) shows trends between actuation lengths and fingertip forces. Similar to Fig. 2(a), fingertip forces for the larger object tends to increase faster and to have higher peak value. Fig. 2(c) shows non-linear behaviors between flexion wire tension and fingertip forces. It is notable that the shape of

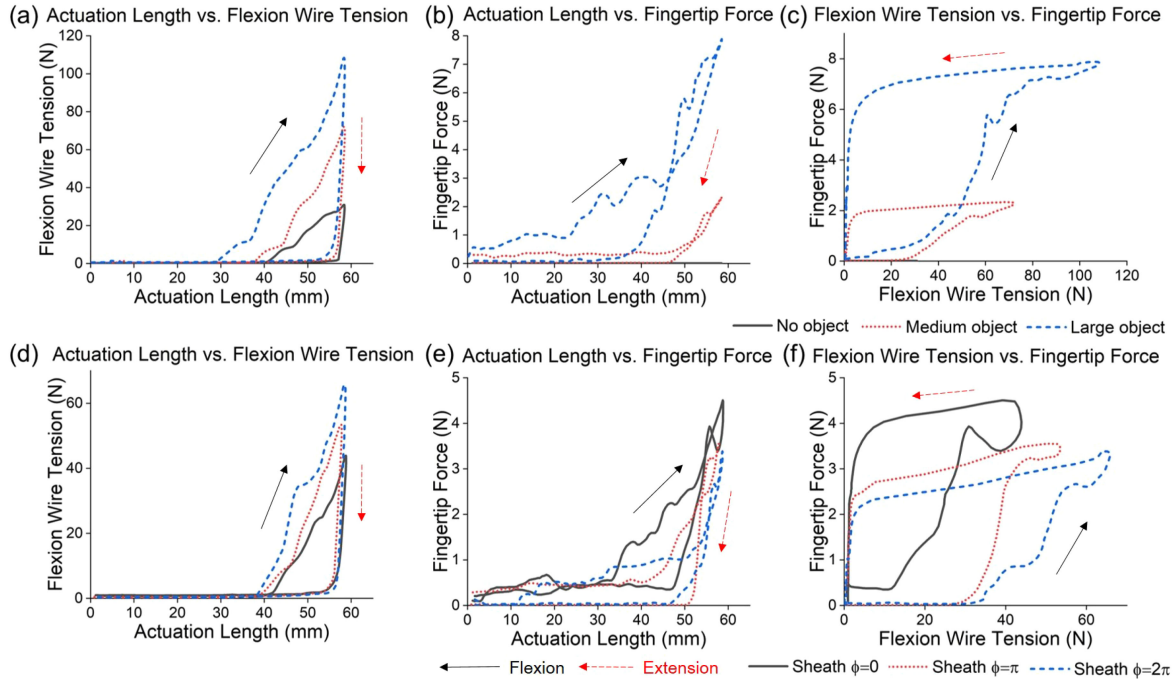


Fig. 2. Non-linear behavior between actuation lengths, flexion wire tension and fingertip forces for varying object sizes and sheath bending angles. Varying objects: (a) Actuation length vs. Flexion wire tension, (b) Actuation length vs. Fingertip force, (c) Flexion wire tension vs. Fingertip force. Varying sheath angles: (d) Actuation length vs. Flexion wire tension, (e) Actuation length vs. Fingertip force, (f) Flexion wire tension vs. Fingertip force.

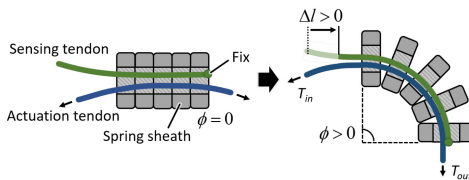


Fig. 3. Concept of embedded BoASensing for bending sensing of TSM.

the loop is different for different object sizes. Here, slopes of the graph for flexion constantly changes as wire tension increases.

2) *Varying Sheath Angles*: Fig. 2(d)–(f) show non-linear behaviors between parameters according to different sheath bending angles when the object size and the actuation length are fixed. For comparison, sheath bending angles were fixed to  $0^\circ$ ,  $180^\circ$  and  $360^\circ$ . Fig. 2(d) shows non-linear trends between actuation lengths and flexion wire tension. As sheath bending angles increase, flexion wire tension increases for the same actuation length. Since wire tension is measured at the actuation system, this phenomenon is explainable in that the friction of TSM also increases as sheath bending angles increase. For the same reason, increased friction in TSM resulted in decreased fingertip forces given same actuation lengths as shown in Fig. 2(e). Fig. 2(f) shows non-linear behaviors between flexion wire tension and fingertip forces. For different sheath bending angles, hysteresis loops have clearly shown to have different trends. In Fig. 2(f), fingertip force drops were observed when flexion wire tension is increased, especially for the case when sheath bending angle is  $0^\circ$ . There are several possible reasons to explain this behavior, such as the change in glove placement relative to the hand, wire path change during actuation, or finger slip on the object during

grasping. In reality, these are the factors that cannot be prevented or controlled, thus making it complicated to estimate fingertip forces.

### III. METHODS

#### A. Hardware Setup

1) *Overall System*: Experiments have been conducted using Exo-Glove Poly II [5], [6] with the customized actuation system. The actuation system consisted of two linear actuators (L16 s, Actuonix, Canada) for flexion and extension. For each actuator, a linear potentiometer, wire length adjuster, loadcell, and BoASensor [24]–[26] were assembled. The role of linear actuators was to pull the wires in the sheaths to transmit wire tension to the glove. Two actuators were operated antagonistically: when the flexion actuator pulls the flexion wire, the extension actuator pushes the extension wire, and vice versa. Linear potentiometers (SoftPot, Spectra Symbol, USA) were located collinear with the direction of the actuators to measure actuation lengths. Wire length adjusters were connected in between the end of the actuators and the wires in order to customize initial wire lengths of Exo-Glove Poly II. To measure wire tension on the flexion and extension wires, loadcells (333LBS, Ktoyo, Korea) were located between the end of the sheaths and the wire length adjusters. At the end of the actuators, BoASensors were assembled to measure sheath bending angles.

Grasping force was measured using a custom-made hand dynamometer as shown in Fig. 1. The dynamometer consisted of four components: Two body structures, spacers, and a loadcell. Two body structures were 3D-printed (Uprint, Stratasys, USA) and were designed in saddle-shape for easy contacts of the

fingers. A loadcell was placed between the structures. In order to change the size of the dynamometer, acrylic plates with 5mm thickness were used as spacers and were placed between a loadcell and one of the structures. For the study, object size numbers in Chapter IV corresponds to the number of spacers placed in the dynamometer. Thus, the sizes of the dynamometer, the distance between the thumb and index finger, are 68mm, 73mm, 78mm, 83mm, and 88mm, for object 1 to 5, respectively.

2) *BoASensor*: As previously mentioned, the sheath bending angle of TSM is one of the most significant parameters that affects the frictional non-linearity of the transmission system. To tackle the issue, BoASensor, which can be placed alongside with the actuation wire inside the sheath, has been proposed to directly measure the sheath bending angles. In detail, two wires, an actuation wire and a sensing wire, were aligned parallel inside the sheaths. BoASensor is working in principle by measuring the displacement change of the sensing wire caused by accumulated bending angles along the sheath. This is because the central displacement of the sheath increases with bending due to geometrical characteristics as illustrated in Fig. 3. Thus, the sensing tendon should be placed only inside the sheaths. Therefore, unlike the actuation tendons, one end of the sensing tendon is installed at the BoASensor module, which is placed at the actuation side end of the sheath. The other end of the sensing tendon installed at the glove side end of the sheath.

### B. Data Collection

The experimental environment to acquire training and testing data sets is shown in Fig. 1. A user, equipped with Exo-Glove Poly II on a desk, was asked to relax and release the user's hand during experiments. For each cycle, grasping of the wearable robot was performed for about 2.0–3.0 seconds, depending on the angular distance, and full release was lasted for 1.5 seconds. During grasping, commanded end-point encoder values for the flexion actuator were randomly assigned with uniform distribution in order for the output fingertip forces to have the values between 5 to 16 Newtons during firm grasp. End-point encoder values for both flexion and extension actuators were manually defined to have the glove fully extended. During data collections, we randomly relocated the sheath by wiring and unwiring it to obtain various range of sheath bending angle data. There were 5 different object sizes, and 50 grasping-and-releasing trials were performed for each object size. Data are sampled at 80Hz. 40 trials for each object were used as training and validation data, and 10 trials for each object were used as testing data.

### C. Fingertip Force Learning

The objective here is to obtain a fingertip force estimation model  $f$  as in

$$\hat{y} = f(x|\theta)$$

where  $\theta$  and  $\hat{y}$  represent parameters to be learned and estimated fingertip forces at the current time  $t$ , respectively. Due to the sequential characteristics of the input data, given problem is usually solved by using Long Short-Term Memory (LSTM). LSTM is a type of Recurrent Neural Network (RNN) structure that has input, forget, and output gates. The forget gate decides what information to keep or discard by multiplying 1 or 0 using a sigmoid unit. These gates enable the network to better deal with

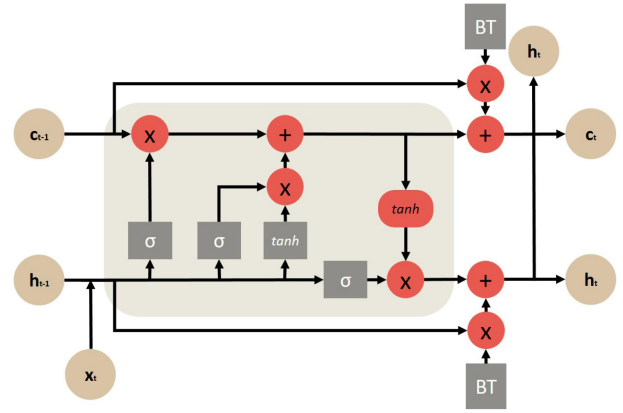


Fig. 4. Bending time-gradient long-short term memory (BT-LSTM).

long-range dependencies caused by the vanishing and exploding gradient problems [28]. LSTM structures are widely used because they are known to be more effective than RNNs [29]. However, due to the fact that fingertip forces greatly depend on bending angles and its changes, a regular LSTM is not able to enumerate accurate fingertip forces. In this paper, BT-LSTM (Bending Time-gradient LSTM), a variant of LSTM, is proposed to deal with such issue.

1) *Input and Output Data*: In a LSTM window with the assigned time window value  $T$ , an input data  $x_t$  at each time step  $t$ , where  $t = 1, 2, \dots, T$ , is composed as follows:

$$x_t = \{x_t^{(1)}, x_t^{(2)}, x_t^{(3)}, x_t^{(4)}, x_t^{(5)}, x_t^{(6)}, x_t^{(7)}, x_t^{(8)}\}$$

where

- 1: Grasping/releasing state
- 2: Movement state (static vs. moving)
- 3: Commanded motor encoder value
- 4: Current motor encoder value
- 5: Tension value on the flexion wire
- 6: Tension value on the extension wire
- 7: Sheath bending angles on the flexion wire
- 8: Sheath bending angles on the extension wire

and  $y_T$  is the fingertip force at time  $T$ . A sequence of the sensor output  $x_{(1:T)} = \{x_{(t=1)}, x_{(t=2)}, \dots, x_{(t=T)}\}$ .

2) *BT-LSTM*: BT-LSTM (Bending Time-gradient LSTM) comprises an additional bending-time gradient residual structure along with a usual LSTM model. This residual structure is to better deal with the change in bending angles from previous states so as to obtain accurate fingertip force values. It aims to obtain cell vector  $c_t \in \mathbb{R}^n$  and output vector  $o_t \in \mathbb{R}^n$  by using the following operations:

$$f_t = \sigma(W_f x_t + U_f h_{t-1} + b_f)$$

$$i_t = \sigma(W_i x_t + U_i h_{t-1} + b_i)$$

$$o_t = \sigma(W_o x_t + U_o h_{t-1} + b_o)$$

$$c'_t = f_t \circ c_{t-1} + i_t \circ \tanh(W_o x_t + U_o h_{t-1} + b_o)$$

$$h'_t = o_t \circ \tanh(c_t)$$

$$BT = \left( \nabla x_t^{(7)} \cdot \frac{t_i}{T} \right)^{\rho_t}$$

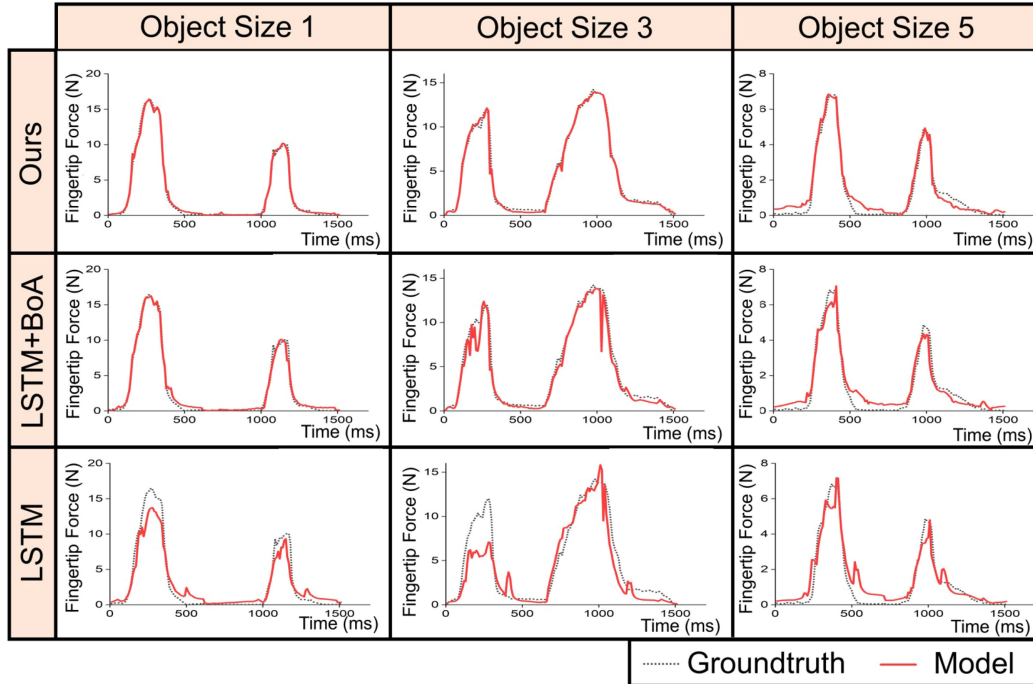


Fig. 5. Results of fingertip force estimation for three different object sizes using BT-LSTM, LSTM+BoA, and LSTM.

$$c_t = c'_t + BT \cdot c_{t-1}$$

$$h_t = h'_t + BT \cdot c_{t-1}$$

where  $\sigma(\cdot)$  and  $\tanh(\cdot)$  respectively denote the element-wise sigmoid and hyperbolic tangent activation functions, and  $\circ$  is an element-wise multiplication.  $i_t \in \mathbb{R}^n$ ,  $f_t \in \mathbb{R}^n$ , and  $o_t \in \mathbb{R}^n$  represent input, forget, and output gates, respectively.  $W_o$ ,  $U_o$ , and  $b_o$  are training parameters for each gate. Unlike the usual LSTM architecture, the BT term in BT-LSTM calculates the gradient of bending angle at the flexion wire given time,  $\nabla x_t^{(7)}$ , which can be obtained by  $x_t^{(7)} - x_{t-1}^{(7)}$ . This term is then multiplied by  $\frac{t_i}{T}$  where  $t_i$  represents the current time index in the time window.  $\rho_t$  is a trainable power term that deals with the non-linearity of the BT term. The overall architecture is depicted in Fig. 4.

3) *Training and Testing*: To train fingertip forces from input data, a three-layer BT-LSTM with 128 hidden units is used. Sequence time length of BT-LSTM was set to  $T = 40$ . The final output of the BT-LSTM layer is fed into the final fully-connected layer to obtain the one-dimensional output. The mean squared error (MSE) function is used to measure the loss between the predicted and the ground truth contact force. During training, the number of epoch was 2000, and the mini batch size was 32. Adam optimizer was used with 0.001 learning rate and  $10^{-5}$  weight decay.

#### IV. RESULTS AND ANALYSIS

BT-LSTM is evaluated by comparing with the performance obtained from three-layer LSTM models with and without bending angle information, abbreviated as LSTM+BoA and LSTM, respectively. To evaluate the performance of the models, Root

TABLE I  
RESULTS OF FINGERTIP FORCE ESTIMATION

	MAE (N)	RMSE (N)
LSTM	0.646	1.119
LSTM+BoA	0.361	0.596
Ours	<b>0.246</b>	<b>0.416</b>

Mean Squared Error (RMSE), Mean Absolute Error (MAE), and Mean Absolute Percentage Error (MAPE) are used.

##### A. Fingertip Force Estimation

The results of the testing errors are shown in Table I. The proposed model had MAE of 0.246N and RMSE of 0.416N. The LSTM model with bending angle information, LSTM+BoA, achieved MAE of 0.361N and RMSE of 0.596N. The regular LSTM without bending angle information gave MAE of 0.646N and RMSE of 1.119N. The model without bending angle information, giving the highest errors amongst all, seems that it fails to accurately obtain contact force of the wearable robot hand. While LSTM+BoA had better accuracy than LSTM, its errors was 46.7% and 43.2% higher than the errors of BT-LSTM in MAE and MSE.

While deep learning methods are known to be good at dealing with hysteresis and non-linearity [23], [30], the LSTM model without having bending angle information is not able to accurately estimate fingertip forces. This can be because the force depends on both the magnitude and change of sheath bending angle of TSM for the soft wearable hand robots. While LSTM+BoA, utilizing bending angle information, has reasonable performance over all objects, it sometimes overshoots or undershoots the peak fingertip force values. On the other hand, it is notable that BT-LSTM shows stable performance over all different object

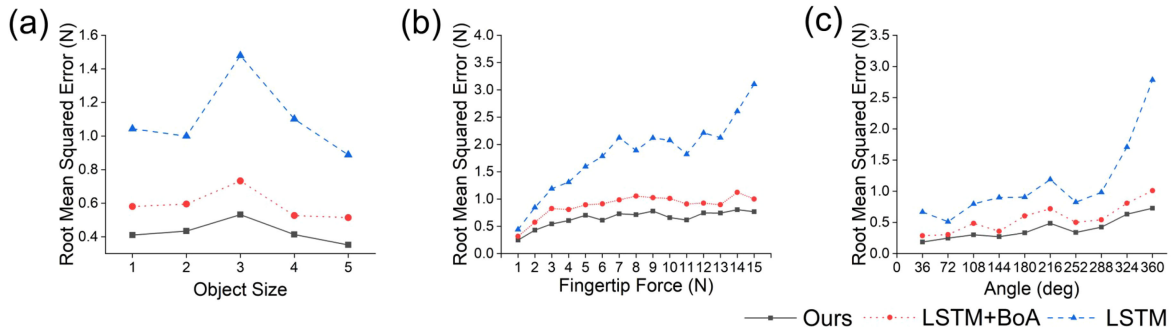


Fig. 6. (a) Root Mean Squared Error of BT-LSTM, LSTM+BoA, and LSTM for different object sizes. (b) Root Mean Squared Error of BT-LSTM, LSTM+BoA, and LSTM for different angular ranges. (c) Root Mean Squared Error of BT-LSTM, LSTM+BoA, and LSTM for different fingertip force ranges.

scenarios. Fig. 5 shows results of the estimated fingertip forces using three different models for different object sizes.

### B. Further Analysis 1: Different Object Sizes

To further analyze the performance of the models, error values for different object sizes were compared as depicted in Fig. 6(a). Based on the results, the proposed model showed the lowest RMSE for all different object sizes. LSTM+BoA had the higher errors than BT-LSTM but lower than LSTM. The best-case scenario of BT-LSTM was when the object size was 5 as the error was 0.35N. When the object size was 3, which was the worst-case, RMSE was 0.53N; RMSE values for LSTM+BoA and LSTM were 0.73N and 1.48N. It is presumed that object 3 could have a lot of confused data points from the neighboring object sizes, compared to other objects because the differences in object size are small.

### C. Further Analysis 2: Different Bending Angle Ranges

An additional test was performed to see how the amount of bending angles at the end point of the time window ( $t = T$ ) affects the corresponding fingertip forces. Fig. 6(b) shows RMSE over different bending angles. Each of the annotated angle values on the x-axis in the figure represents angle range between the value and the previously-annotated value. Based on the result, as bending angles increased, the error of the overall models tended to be increased. In other words, when the sheath of the robot is curvier, it is harder to estimate accurate fingertip forces. However, in comparison with other models, BT-LSTM provided better results over all angular ranges. When the angle was in between  $324^\circ$  and  $360^\circ$ , which was the worst-case scenario, BT-LSTM had RMSE of 0.73N while LSTM+BoA and LSTM had 1.01N and 2.78N errors in RMSE, respectively.

### D. Further Analysis 3: Different Force Ranges

Fig. 6(c) shows RMSE over the different range of ground truth fingertip forces. Each of the annotated fingertip force values on the x-axis in the figure represents the fingertip force range between the value and the previously-annotated value. The error of the estimated contact force increases as the ground truth contact force increases for all models. It may be rational that the larger absolute value, the more error. Still, BT-LSTM outperforms the other models over all range of ground truth fingertip forces. For the worst-case scenario (when the force

range is in between 13 and 14N), RMSE of BT-LSTM was 0.80N while LSTM+BoA and LSTM had RMSE of 1.12N and 2.61N.

### E. Further Analysis 4: Bending Angle Changes During Grasping

In this section, to verify the performance of the proposed model in the situation where bending angle continuously changes, the sheaths were manually manipulated during data gathering. The result, depicted in Fig. 7, shows that BT-LSTM was able to estimate fingertip forces under continuous bending angle changes. On the other hand, other two models did not seem to produce accurate results compared to BT-LSTM.

To quantitatively analyze the impact of dynamic angle changes, the top 5,000 data that had the largest cumulative bending angle changes and the smallest cumulative bending angle changes were compared in RMSE. The cumulative changes in bending angle were calculated by  $\sum_{t=2}^T |x_t^{(7)} - x_{t-1}^{(7)}|$ . The proposed model had 0.26 N (top 5,000 smallest) and 0.44 N (top 5,000 largest). LSTM+BoA had 0.32 N (smallest) and 0.75 N (largest). LSTM did not seem to produce accurate results for both smallest and largest changes in bending angle, which had 0.99 N (smallest) and 1.1 N (largest). Based on the result, the proposed method had the less impact of the bending angle changes compared to LSTM+BoA.

### F. Further Analysis 5: Repeatability

In order to evaluate the repeatability, additional experiments were performed to gather three different test datasets. Each of the test datasets was collected 1) in accordance with the aforementioned data collection method, 2) on a different day, and 3) by re-assembling the actuation system. The results are tabulated in Table II. The performance of the proposed method was slightly decreased from 0.246N in MAE and 0.416N in RMSE to 0.287N in MAE and 0.462N in RMSE. However, the other two methods show severe performance degradation. The performance of LSTM+BoA was decreased from 0.361N in MAE and 0.596N in RMSE to 0.719N in MAE and 0.971N in RMSE. Standard deviations of the absolute errors for each method were also displayed. BT-LSTM had the standard deviation of 0.362N while LSTM+BoA and LSTM had the standard deviations of 0.971N and 1.517N, respectively.

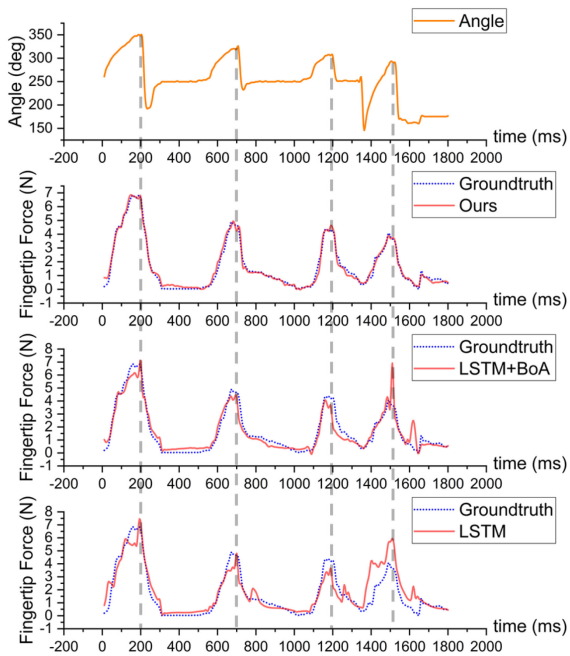


Fig. 7. Fingertip force estimation results using BT-LSTM, LSTM-BoA, and LSTM during constant angle change.

TABLE II  
RESULTS OF FINGERTIP FORCE ESTIMATION FOR REPEATABILITY

	MAE (N)	STDV (N)	RMSE (N)
LSTM	2.041	1.517	2.543
LSTM+BoA	0.719	0.971	1.208
Ours	<b>0.287</b>	<b>0.362</b>	<b>0.462</b>

### G. Further Analysis 6: Real-time Applicability and Force Control

This section is to examine the feasibility for an actual deployment of the proposed system. Two computing devices were tested for real-time applicability: a laptop (ROX Zephyrus GX501, Asus) and an embedded computing device (Jetson AGX Xavier, NVIDIA). On the laptop, the fingertip forces were estimated with 125 Hz, and the embedded device gave 22.2 Hz.

To validate that the proposed system enables force control, a PID controller was implemented and tested under the laptop setting. The controller was tested using a 5-second step function as input signals, as shown in Fig. 8. MAE between the desired and measured force was 0.72N, which is 12.7% in MAPE. The desired force has been reached in about 1.2 seconds while it takes about 1.4 seconds to return back to the rest. Compared to Hofmann *et al.* [22], whose performance was 6.6% in MAPE for the step response, this error seems a bit higher although they used a different actuation system. It is assumed that the biggest error of the proposed method is due to the slower actuation system; the time taken to the force setpoint was more than twice as slow as Hofmann *et al.* It is notable that after reaching the desired force, MAE became 0.31N, which is 3.69% in MAPE.

## V. DISCUSSION AND CONCLUSION

This paper proposed a deep learning-based method for estimating fingertip forces by using motor encoders, wire tension and bending angle information. The actuation system included

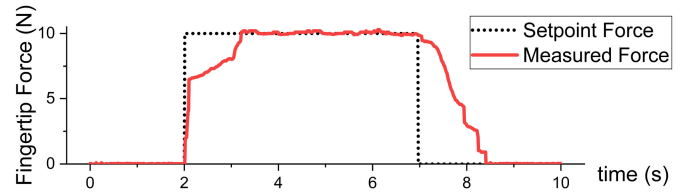


Fig. 8. Force control results using the step function.

sensors to measure wire tension and actuation lengths. To measure sheath bending angles, BoASensors were embedded in the actuation system. Exo-Glove Poly II, a soft under-actuated tendon-driven wearable robot, was used to verify the proposed method. Existing problems that hinder to measure fingertip forces, including non-linearity, hysteresis and the influence of bending angles were presented. To deal with the aforementioned, BT-LSTM, a modified version of LSTM, was presented. The performance of BT-LSTM was evaluated by comparing with regular LSTM models including and excluding sheath bending angle information as inputs. This paper further analyzed the performance of the proposed model by using different object sizes and analyzing how sheath bending angles and fingertip forces affected the model's error. Then, the repeatability test was performed using three different datasets collected on different days. To validate the possibility of actual deployment, portable devices were tested. The ability of force control using the proposed method is also examined.

The results showed that the proposed approach was accurately able to estimate fingertip forces under various criteria like different object sizes and angular disturbances in comparison with an existing model. This suggests that the sheath bending angle is an important factor to estimate fingertip forces for soft wearable hand robots with TSM. The robots are known to have non-linearity and hysteresis on both proximal and distal end. In addition, when measuring fingertip forces from wire tension, their fingertip forces are greatly influenced by dynamic changes of the sheath bending angle. This problem was alleviated by designing an extra residual module that integrates sheath bending angle information and time gradient.

Although the proposed method outperformed the other learning-based models in estimating fingertip forces, there still are some limitations and challenges that need to be further developed. First, the proposed method needs vast calculations during inferences compared to existing non-deep-learning-based methods. For force control, this study used the laptop as a computing device, which is small enough to fit in wheelchairs. However, since the computation speed of the embedded devices were not fast enough, this kind of task may not currently be manageable. Second, the proposed method is data-dependent. It requires a lot of data for training the network and takes long training time. To overcome this, integrating the proposed approach with a prior knowledge using existing methods [22] would be necessary.

A future work can be to consider non-rigid objects when measuring fingertip forces. While this being an important issue to solve, softness of non-rigid objects can create another complexity and non-linearity when estimating fingertip forces through measuring wire tension and sheath bending angles. Furthermore, The proposed method can be used to manage other non-linear behaviors by using BT term of the algorithm. Thus, in the future, the proposed method has potential to be implemented into any robotic systems that uses remote actuation systems with TSM, such as medical robots.

## REFERENCES

- [1] P. Polygerinos, Z. Wang, K. C. Galloway, R. J. Wood, and C. J. Walsh, "Soft robotic glove for combined assistance and at-home rehabilitation," *Robot. Autom. Syst.*, vol. 73, pp. 135–143, 2015.
- [2] N. Cheng, J. H. Low, B. W. K. Ang, A. J. Y. Goh, and C. Yeow, "Soft fabric-based pneumatic sensor for bending angles and contact force detection," *IEEE Sensors*, vol. 19, no. 4, pp. 1269–1279, Feb. 2019.
- [3] H. In, B. B. Kang, M. Sin, and K. Cho, "Exo-Glove: A wearable robot for the hand with a soft Tendon routing system," *IEEE Robot. Autom. Mag.*, Vol. 22, no. 1, pp. 97–105, Mar. 2015.
- [4] B. B. Kang, H. Lee, H. In, U. Jeong, J. Chung, and K. Cho, "Development of a polymer-based Tendon-driven wearable robotic hand," in *Proc. IEEE Int. Conf. Robot. Autom.*, 2016, pp. 3750–3755.
- [5] B. B. Kang, H. Choi, H. Lee, and K. -J. Cho, "Exo-glove poly II: A polymer-based soft wearable robot for the hand with a Tendon-driven actuation system," *Soft Robot.*, vol. 6, no. 2, pp. 214–227, 2019.
- [6] D. Kim *et al.*, "Eyes are faster than hands: A soft wearable robot learns user intention from the egocentric view," *Sci. Robot.*, vol. 4, no. 26, 2019, Art. no. eaav2949.
- [7] D. Popov, I. Gaponov, and J. Ryu, "Portable exoskeleton glove with soft structure for hand assistance in activities of daily living," *IEEE Trans. Mechatronics*, vol. 22, no. 2, pp. 965–975, Apr. 2017.
- [8] M. Nilsson, J. Ingvast, J. Wikander, and H. Von Holst, "The soft extra muscle system for improving the grasping capability in neurological rehabilitation," in *Proc. IEEE-EMBS Conf. Biomed. Eng. Sci.*, Dec. 2012, pp. 412–417.
- [9] L. Randazzo, I. Iturrate, S. Perdakis, and J. D. R. Millan, "Mano: A wearable hand Exoskeleton for activities of daily living and Neurorehabilitation," *IEEE Robot. Autom. Lett.*, vol. 3, no. 1, pp. 500–507, Jan. 2018.
- [10] C. J. Nycz, T. Butzer, O. Lamercy, J. Arata, G. S. Fischer, and R. Gassert, "Design and characterization of a lightweight and fully portable remote actuation system for use with a hand Exoskeleton," *IEEE Robot. Autom. Lett.*, vol. 1, no. 2, pp. 976–983, Jul. 2016.
- [11] S. Sundaram, P. Kellnhofer, Y. Li, J. Zhu, A. Torralba, and W. Matusik, "Learning the signatures of the human grasp using a scalable tactile glove," *Nature*, vol. 569, pp. 698–702, 2019.
- [12] P. S. Girao, P. M. P. Ramos, O. Postolache, J. Miguel, and D. Pereira, "Tactile sensors for robotic applications," *Measurement*, vol. 46, no. 3, pp. 1257–1271, 2013.
- [13] Y. Wang, K. Xi, D. Mei, Z. Xin, and Z. Chen, "Three-axis contact force measurement of a flexible tactile sensor array for hand grasping applications," *Wearable Sensors Robots*, vol. 399, pp. 67–79, 2017.
- [14] E. Battaglia *et al.*, "ThimbleSense: A fingertip-wearable tactile sensor for grasp analysis," *IEEE Trans. Haptics*, vol. 9, no. 1, pp. 121–133, Jan.–Apr. 2015.
- [15] H. Kristanto, P. Sathe, A. Schmitz, T. P. Tomo, S. Somlor, and S. Sugano, "A wearable three-axis tactile sensor for human fingertips," *IEEE Robot. Autom. Lett.*, vol. 3, no. 4, pp. 4313–4320, Oct. 2018.
- [16] E. Hocaoglu, "WeFiTS: Wearable fingertip tactile sensor," in *Proc. Int. Symp. Wearable Robot.*, 2018, pp. 28–32.
- [17] G. D. Pasquale, L. Mastrototaro, L. Pia, and D. Burin, "Wearable system with embedded force sensors for neurologic rehabilitation trainings," in *Proc. Symp. Des., Test, Integration Packag. MEMS MOEMS*, 2018, pp. 1–4.
- [18] M. Mohammadi, T. L. Baldi, S. Scheggi, and D. Prattichizzo, "Fingertip force estimation via inertial and magnetic sensors in deformable object manipulation," in *Proc. IEEE Haptics Symp.*, 2016, pp. 284–289.
- [19] M. Kaneko, T. Yamashita, and K. Tanie, "Basic considerations on transmission characteristics for tendon drive robots," in *Proc. Int. Conf. Adv. Robot.*, 1991, pp. 827–832.
- [20] G. Palli, G. Borghesan, and C. Melchiorri, "Modeling, identification, and control of Tendon-based actuation systems," *IEEE Trans. Robot.*, vol. 28, no. 2, pp. 277–290, Apr. 2012.
- [21] B. Bardou, F. Nageotte, P. Zanne, and M. de Mathelin, "Improvements in the control of a flexible endoscopic system," in *Proc. IEEE Int. Conf. Robot. Autom.*, 2012, pp. 3725–3732.
- [22] U. A. T. Hofmann, T. Butzer, O. Lamercy, and R. Gassert, "Design and evaluation of a Bowden-cable-based remote actuation system for wearable robotics," *IEEE Robot. Autom. Lett.*, vol. 3, no. 3, pp. 2101–2108, Jul. 2018.
- [23] X. Li, L. Cao, A. M. H. Tiong, P. T. Phan, and S. J. Phee, "Distal-end force prediction of Tendon-sheath mechanisms for flexible endoscopic surgical robots using deep learning," *Mechanism Mach. Theory*, vol. 134, pp. 323–337, Apr. 2019.
- [24] U. Jeong and K.-J. Cho, "A novel low-cost, large curvature bend sensor based on a Bowden-cable," *Sensors*, vol. 16, no. 7, 2016, Art. no. 961.
- [25] U. Jeong and K.-J. Cho, "A feasibility study on tension control of Bowden-cable based on a dual-wire scheme," *IEEE Int. Conf. Robot. Autom.*, 2017, pp. 3690–3695.
- [26] U. Jeong and K.-J. Cho, "Control of a Bowden-cable actuation system with embedded BoASensor for soft wearable robots," *IEEE Trans. Ind. Electron.*, to be published.
- [27] S. Hochreiter and J. Schmidhuber, "Long short-term memory," *Neural Comput.*, vol. 9, no. 8, pp. 1735–1780, 1997.
- [28] Y. Bengio, P. Simard, and P. Frasconi, "Learning long-term dependencies with gradient descent is difficult," *IEEE Trans. Neural Netw.*, vol. 5, no. 2, pp. 157–166, Mar. 1994.
- [29] Y. LeCun, Y. Bengio, and G. Hinton, "Deep learning," *Nature*, vol. 521, no. 7553, pp. 436–444, 2015.
- [30] S. Han, T. Kim, D. Kim, Y.-L. Park, and S. Jo, "Use of deep learning for characterization of microfluidic soft sensors," *IEEE Robot. Autom. Lett.*, vol. 3, no. 2, pp. 873–880, Apr. 2018.